

Molecular insight into hydrogen storage in clathrate hydrates: The effect of different promoters on the spontaneous nucleation of hydrogen hydrates studied via microsecond-scale molecular dynamics simulations

Fengyi Mi^{a,b} , Fulong Ning^{a,*} , Thijs J.H. Vlugt^b, Othonas A. Moultsos^{b,*}

^a National Center for International Research on Deep Earth Drilling and Resource Development, Faculty of Engineering, China University of Geosciences, Wuhan, Hubei 430074, China

^b Engineering Thermodynamics, Process & Energy Department, Faculty of Mechanical Engineering, Delft University of Technology, Leeghwaterstraat 39, Delft 2628CB, the Netherlands

ARTICLE INFO

Keywords:

Hydrogen storage
Molecular dynamics simulation
Binary hydrogen hydrate
Hydrogen hydrate nucleation
Hydrate promoters

ABSTRACT

Hydrate-based H₂ storage is based on the mechanism of trapping H₂ in water-based structures that are environmentally friendly and cost-efficient. Understanding the effects of common promoters on hydrate-based H₂ storage at the molecular level is crucial for designing efficient storage systems, and for discovering novel promoters. Here, a series of μs-scale molecular dynamics simulations are performed to investigate the nucleation of binary H₂ hydrates from gas-liquid two-phase solutions in the presence of various promoters, *i.e.*, CH₄, CO₂, C₂H₆, C₃H₈, C₅H₁₀, and THF. The simulation results indicate that the H₂ and promoter molecules first dissolve in water from the gas phase and then are absorbed on the cage-faces, promoting the nucleation and growth of binary H₂ hydrates. THF is the most effective promoter for hydrate-based H₂ storage, exhibiting high performance in converting H₂ from the gas phase to hydrates. It is followed by CH₄, C₂H₆, and CO₂; C₃H₈ and C₅H₁₀ molecules are less effective H₂ hydrate promoters. The presence of large promoter molecules enhances multi-occupied cage formation. The molecular insight into the nucleation of binary H₂ hydrates with various promoters provided here not only contributes to a broader understanding of hydrate-based H₂ storage but is expected to motivate further experimental and computational studies.

1. Introduction

Hydrogen (H₂) is anticipated to play a pivotal role in the global energy transition [1]. H₂ has high gravimetric energy density, while H₂ combustion produces only water, which is promising for enabling near-zero emission technologies. However, to efficiently and safely store and transport H₂, many technical challenges should be overcome. Although H₂ can be stored in different physical and chemical ways (*e.g.*, liquefaction [2], compression [3], 2D materials [4,5], porous materials [6], and metal hydrides [7]), most of these have disadvantages such as large energy consumption, strict operating conditions, high cost, and possible hazards owing to the low volumetric density (0.08 g/L) and high flammability of H₂ [8,9]. A promising alternative is hydrate-based H₂ storage, *i.e.*, H₂ is encapsulated in water-based structures (clathrate hydrates) that operate at relatively mild conditions compared to other storage methods, *e.g.*, liquefaction [10–12]. Since clathrate hydrates are

formed by the directional arrangement of water molecules, they are a class of sustainable and environmentally friendly nanomaterials capable of H₂ storage [13–18].

The relatively high pressures required for the formation of pure H₂ hydrate combined with their slow formation rates, hinder the large-scale implementation of hydrate-based H₂ storage [19–21]. To this end, in the past few decades, considerable efforts have been made to enhance the formation kinetics of H₂ hydrates and alleviate the formation conditions [22–30]. Promoters such as methane (CH₄), carbon dioxide (CO₂), ethane (C₂H₆), propane (C₃H₈), tetrahydrofuran (THF), and cyclopentane (C₅H₁₀), have been shown to significantly change the phase equilibrium of H₂ hydrates [31–35]. These molecules can form binary hydrates with H₂, where they mainly occupy large cages, while H₂ occupies small cages [36,37]. The experimental results of Lee and co-workers [10] show that THF molecules occupy large cages to stabilize the binary H₂ hydrate structure, thereby, reducing the pressure

* Corresponding authors.

E-mail addresses: nflzx@cug.edu.cn (F. Ning), o.moultsos@tudelft.nl (O.A. Moultsos).

conditions for H₂ storage from 200 MPa to 12 MPa. A drawback is that the formation of binary hydrates reduces H₂ storage capacity due to the occupation of large cages by the promoters. Numerous experimental studies have sought to balance H₂ storage capacity and H₂ storage efficiency from promoter species, promoter concentration, temperature, pressure, and other factors [38–43]. Nevertheless, experimental approaches lack molecular resolution, and therefore, cannot observe, and thus, provide physical insights into the underlying mechanisms of binary H₂ hydrate nucleation and growth.

Access to the nanoscale is essential for understanding the influence of promoters on binary hydrate formation kinetics and H₂ storage capacity. To this purpose, molecular simulation, and Molecular Dynamics (MD) simulation in particular, is the natural tool for elucidating the formation process of H₂ hydrates at the molecular level [44–48]. Alavi and co-workers [44] performed MD simulations and showed that the most stable hydrate crystal structures occur when a single H₂ molecule occupies a small cage, and four H₂ molecules occupy a large cage. Wang *et al.* [49–51] performed a series of MD simulations to study the formation of binary H₂-propane hydrates under different pressures and promoter concentrations. Fan *et al.* [52] showed that the H₂ storage capacity in a clathrate hydrate is mainly affected by temperature. Several other MD studies explored the influence of environmental factors on the storage capacity of H₂ hydrates with various promoters, such as CH₄, CO₂, THF, and C₃H₈ [53–56]. Although prior MD studies mainly focused on H₂ hydrate growth and binary H₂ hydrate nucleation from homogeneous solutions with very high H₂ concentrations, hydrate nucleation usually occurs at the gas-liquid interface. The exact nucleation mechanisms of H₂ hydrate from gas-liquid two-phase solutions with promoters still remain obscure despite being crucial for developing hydrate-based H₂ storage.

In this study, for the first time in hydrate-related literature, an extensive series of MD simulations are performed to investigate the nucleation mechanisms of binary H₂ hydrates from gas-liquid two-phase solutions in the presence of various promoters, *i.e.*, CH₄, CO₂, C₂H₆, C₃H₈, C₅H₁₀, and THF. By performing μ s-scale MD simulations, we observe that H₂ and promoter molecules first dissolve in water from the gas phase and then are absorbed on the cage-faces, promoting the nucleation and growth of binary H₂ hydrates. Our results clearly show that THF is the most effective promoter for hydrate-based H₂ storage, exhibiting high performance in converting H₂ from the gas to hydrates. Our study provides unique molecular insights that can serve as a reference for investigating new promoters, while motivating and guiding further experimental and simulation studies of hydrate-based H₂ storage. This paper is organized as follows: Section 2 provides a short description of the molecular simulation techniques and models. In section 3, the nucleation mechanism of binary H₂ hydrates and the effect of promoter species on hydrate-based H₂ storage are investigated. Concluding remarks are presented in Section 4. Details on the simulations and methods are provided in the Supplementary material.

2. Simulation models and methods

The hydrate nucleation promoters considered here are: CH₄, CO₂, C₂H₆, C₃H₈, C₅H₁₀, and THF (Fig. S1). These hydrate nucleation promoters frequently appear in previous experimental literature [31–35], because pure H₂ does not form hydrates under the selected conditions, while the addition of these promoter molecules facilitates the nucleation and growth of binary H₂ hydrates. A system of pure H₂ was also studied as a reference. Thus, seven systems in total were tested. Hereafter, these systems are referred to as H_{Pure}, H_{CH4}, H_{CO2}, H_{C2H6}, H_{C3H8}, H_{C5H10}, and H_{THF}. Details on the composition of these systems are listed in Table S1. Each system comprised 300 H₂, 180 promoter, and 3060 H₂O molecules. The number ratio of H₂ to promoter molecules is 0.625, which is favorable for binary hydrate formation as shown in the literature [50]. The number ratio of the promoter to H₂O molecules is 17, which is consistent with the ratio of large cages to H₂O molecules in a standard

SII-type hydrate [57]. To obtain statistics four independent simulations were performed for each system, each one starting from a different initial configuration. Nucleation occurred at different times (the so-called induction time) and in a random fashion in each simulation. In all simulations, H₂ hydrates nucleated from the gas-liquid two-phase configuration as shown in Fig. 1 and Fig. S2(a-h) in the Supplementary material. The presence of a gas-liquid interface introduces interfacial tension, which, according to the Laplace equation, results in higher internal pressures in smaller bubbles. This, in turn, can increase the local solubility of H₂ in the aqueous phase. The system sizes in the simulations performed here are relatively small, and although different runs produced some variations in bubble size, the overall statistical analysis of nucleation events showed similar trends across the replicas.

The OPLS-AA force field [58] was used to model the CH₄, C₂H₆, C₃H₈, THF, and C₅H₁₀ molecules. CO₂ and H₂O molecules were modeled using the TraPPE [59] and TIP4P/Ice force fields [60], respectively. For H₂, the three-site model developed by Alavi *et al* [44] was used. All force field details are listed in Tables S3 and S4 in the Supplementary material. Due to the lack of experimental solubility data for H₂ in water under specific conditions, direct comparison is not feasible, but the force fields used here have been widely tested under related conditions. These force fields have been extensively validated in previous studies for their accuracy in predicting hydrate phase behavior [49,50,52–56,61]. The Lorentz-Berthelot mixing rules were used for the cross interactions.

All properties of interest, *i.e.*, free energies, diffusivities, residence time correlation functions, order parameters, hydrogen uptake, were computed from production runs of 3 μ s in the isothermal-isobaric (NPT) ensemble at a pressure of 1100 bar and a temperature of 240 K. The simulation conditions (1100 bar and 240 K) were selected based on prior studies [50,52], where binary H₂ hydrate nucleation was successfully observed, confirming that these conditions fall within the hydrate stability region for relevant systems. In addition, based on the experimental data for the phase equilibrium of single guest molecule hydrates (listed in Table S2 in the Supplementary material), it is evident that the simulation conditions considered here fall into the stable region of binary hydrates. These conditions ensure that the time required for hydrate nucleation is accessible within the molecular simulation, and at a reasonable computational cost. These conditions have also been shown in previous studies to be the most favourable for the nucleation of binary H₂ hydrates [50,52]. To regulate the temperature and pressure, the Nosé-Hoover thermostat [62] and Parrinello-Rahman barostat [63] with time constants of 2 ps and 4 ps, were used, respectively. Periodic boundary conditions were applied in all directions. The simulations were performed using the GROMACS MD simulation package (version 2022) [64]. Details of the simulation methods (*e.g.*, initial configurations, equilibration scheme, electrostatics, timesteps) along with the calculation principles of the properties computed in this study are provided in the Supplementary material.

3. Results and discussion

3.1. Effect of interactions between promoter and H₂O/H₂ molecules on hydrate nucleation

The interactions between promoter and H₂/H₂O molecules play an important role in the nucleation of binary H₂ hydrates, and therefore, also affect H₂ storage. To study the effect of interactions between different promoters and H₂O molecules on hydrate nucleation, the Gibbs free energies (ΔG) of six different promoter molecules in aqueous solution are computed; see Fig. 2(a). Gibbs free energy provides information on the dissolution of the different promoter species in water. The solvation free energy of a gas in water is thermodynamically related to its Henry's constant and can be used to assess gas solubility under a given partial pressure. At the conditions considered here (*i.e.*, 240 K and 110 MPa), experimentally measured Henry's constants are lacking, making comparisons of our data with experiments not possible.

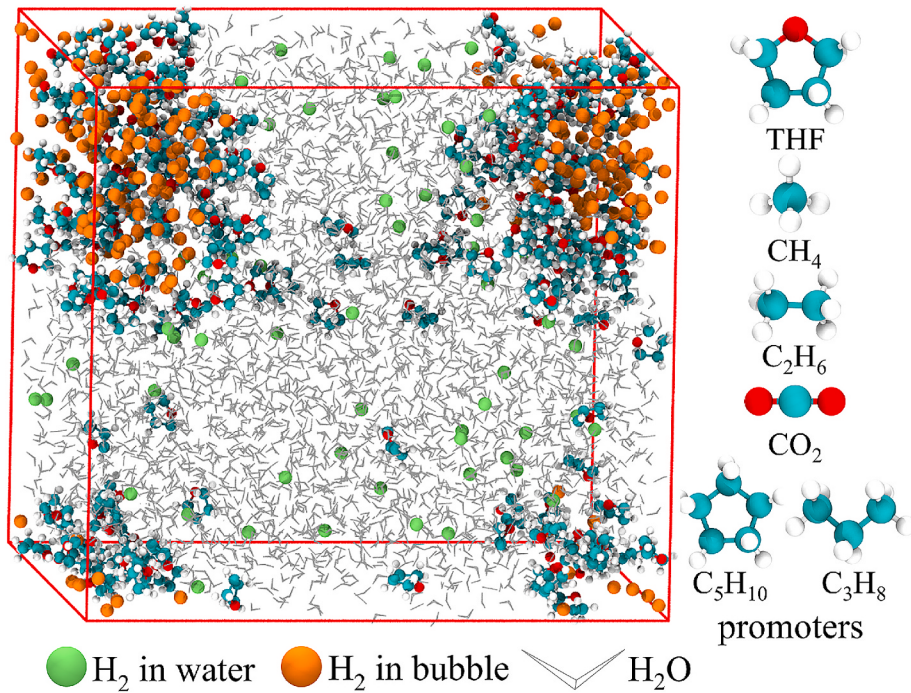


Fig. 1. A representative initial configuration for the MD simulation. The molecular structures of the six promoters are shown on the right. Orange balls, green balls, and silver lines represent H_2 in nanobubble, H_2 in water, and H_2O , respectively. (For interpretation of the references to colour in this figure legend, the reader is referred to the web version of this article.)

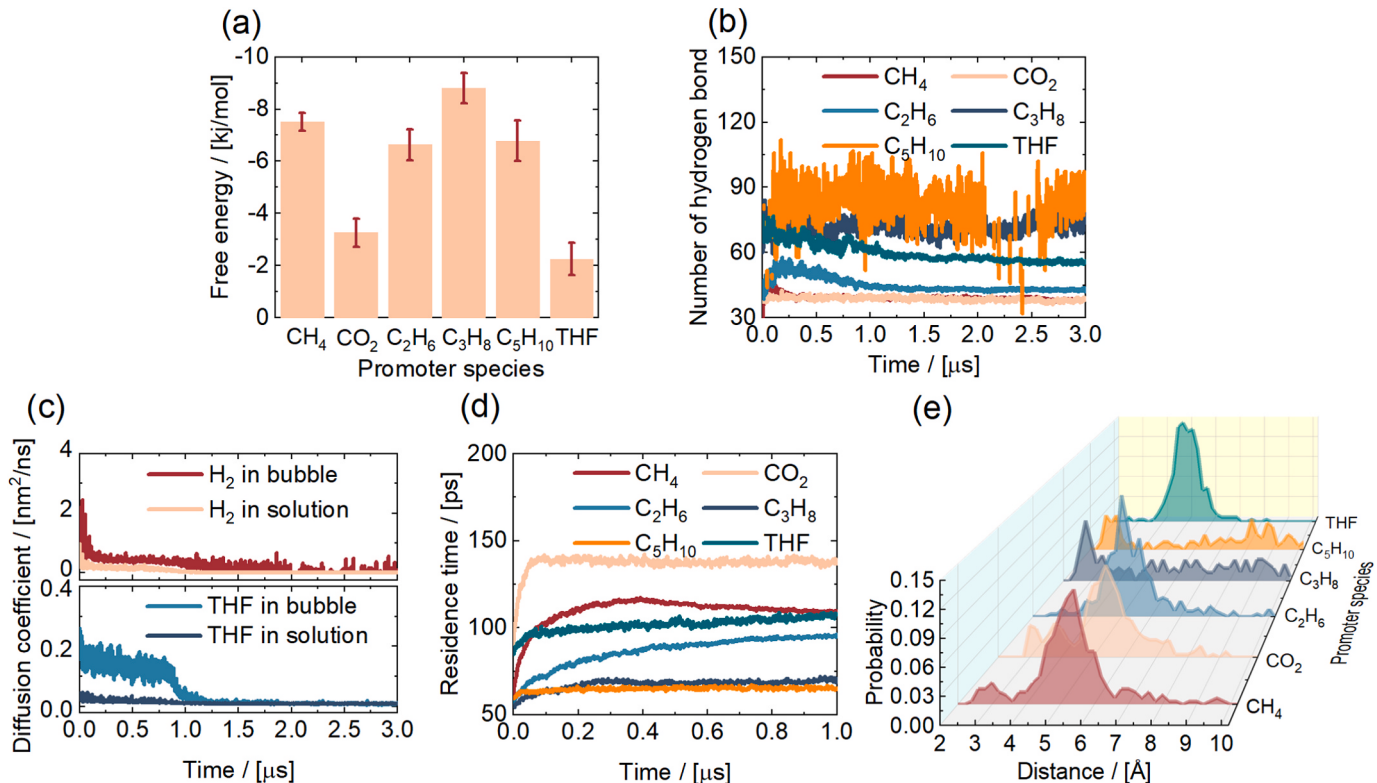


Fig. 2. (a) Gibbs free energies of various promoters in water at 240 K 1100 bar. Time evolution of (b) the number of hydrogen bonds near the promoter molecules in water, (c) the average diffusion coefficient for guest molecules (H_2 and THF) in bubble and solution, (d) the average residence time for H_2O near promoter in water, and (e) probability distribution of the distances between H_2 in water and various promoters at 3 μs .

However, the solvation free energy values calculated in this study are close to the results of previous studies [65]. The lower (*i.e.*, the more negative) the Gibbs free energy, the more thermodynamically

favourable the dissolution process is. This indicates a higher solubility of the species in water, and thus, ΔG can potentially affect the diffusivity of the species in the solvent, *i.e.*, a low ΔG means that the promoter can

diffuse faster in the aqueous solution. As can be seen in Fig. 2(a), C₃H₈ in the solution has the lowest free energy value, and thus, C₃H₈ molecules are expected to diffuse faster in water. This is consistent with the findings by Fang et al. [66], where it is shown that C₃H₈ and CH₄ exhibit high diffusivities in aqueous electrolyte solutions at different temperatures, pressures, and salinities. The high diffusivity of C₃H₈ in water disrupts the hydrogen bond network of water molecules in the vicinity of the promoter molecule, and thus, inhibits hydrate nucleation. As shown in Fig. 2(a), THF exhibits the highest free energy value, suggesting that THF molecules have lower diffusion in water compared to the rest of the promoter molecules studied here. While solvation free energy is correlated with solubility, additional factors such as molecular size, hydration shell structure, and hydrophobic interactions can lead to deviations from experimentally measured solubilities. For example, although CH₄ is less soluble than THF in bulk water, its small molecular size and hydrophobic hydration effects result in a more negative solvation free energy compared to THF as shown in Fig. 2(a). Different promoters affect the hydrogen bonding network formed by surrounding H₂O molecules differently. The time evolution of the number of hydrogen bonds around the promoter in water is shown in Fig. 2(b). The number of hydrogen bonds around C₃H₈ and C₅H₁₀ molecules in water stabilizes at a high value, whereas the hydrogen bonds around CH₄, CO₂, C₂H₆, and THF molecules are fewer and slightly decrease with time (see also Fig. S3(a-f) in the Supplementary material). This complements the direct measurement of diffusivity by providing additional information about the interaction between the promoter and water molecules. Together, these metrics offer a deeper insight into the complex interplay of physical mechanisms involved in the system (see Fig. 2(c), and Fig. S4(a-f) and Fig. S5(a-f) in the Supplementary material).

The mobility of promoter molecules in the hydrogen bonding network has a strong effect on hydrate nucleation [67]. Slow-diffusing promoter molecules are beneficial for the nucleation of binary H₂ hydrates. In our simulations, the promoter molecules can be found in two different states: (1) residing in nanobubbles (*i.e.*, gas phase) or (2) as free molecules dissolved in water (see Fig. 1). As shown in Fig. 2(c), and Fig. S4(a-f) and Fig. S5(a-f) in the Supplementary material, the diffusion

coefficients of promoter molecules in nanobubbles are higher than their diffusivity when dissolved in water. As mentioned earlier, the low diffusivities of promoter and H₂ molecules are favourable for binary H₂ hydrate nucleation.

To further study the influence of promoter molecules on their surrounding H₂O molecules during the binary H₂ hydrate formation, the residence time of H₂O molecules near various promoter molecules is calculated. As can be seen in Fig. 2(d) and Fig. S6(a-f) in the Supplementary material, the residence time for H₂O molecules near C₃H₈ and C₅H₁₀ molecules is lower than that of other promoters. These findings indicate that H₂O molecules are less likely to cluster near C₃H₈ and C₅H₁₀ molecules, which is not favourable for binary H₂ hydrate nucleation, and thus, H₂ storage in clathrate hydrates.

To investigate the strength of interactions between H₂ and promoter molecules, the probability distribution of the distance between H₂ molecules dissolved in water and promoter molecules is computed. At 3 μs of simulation time, the distance probability curve between H₂ in water and promoter species CH₄, CO₂, C₂H₆, and THF shows a peak at a distance of ca. 0.5 nm (Fig. 2(e), and S7(a-f), and S8(a-f) in the Supplementary material). The corresponding distance for C₃H₈ and C₅H₁₀ did not exhibit such peaks (Fig. 2(b), S7(a-f), and S8(a-f)), likely due to the absence of hydrate nucleation during the period of 3 μs.

3.2. Nucleation mechanisms of binary H₂ hydrates

The dissolution of guest (H₂ and promoter) molecules in water, and the absorption of guest molecules on the faces of the hydrate cage (as shown in Fig. 3(a-f)) are crucial for binary H₂ hydrates nucleation. The spontaneous nucleation process of binary H₂-THF hydrates is illustrated in Fig. 4(a-f), where snapshots from the MD simulations at different simulation times are shown. H₂ and THF molecules form mixed hydrate clusters after ca. 0.7 μs of simulation time as can be observed in Fig. 4(a-c). The nucleation process of binary hydrate cages (during 0.615–0.631 μs) is shown in Fig. 3(a-f). Since a hydrate cage is a hydrogen bond cage-like network formed by water molecules surrounding guest molecules, the formation of hydrogen bond networks around guest molecules is

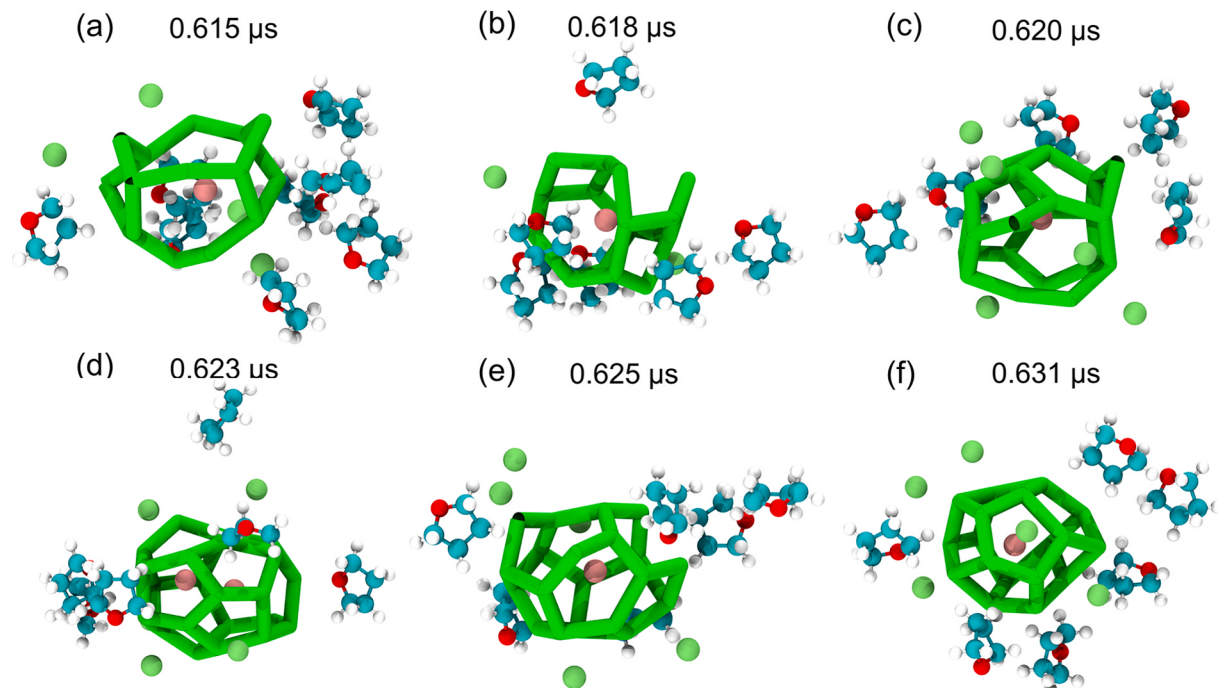


Fig. 3. (a-f) Nucleation process of H₂ hydrate cages in the H₂-THF system. THF molecules are displayed as cyan (C atom), red (O atom), and white (H atom). Pink and green balls represent H₂ in hydrate and H₂ in solution, respectively. Green bonds represent hydrogen bonds formed by water molecules. (For interpretation of the references to colour in this figure legend, the reader is referred to the web version of this article.)

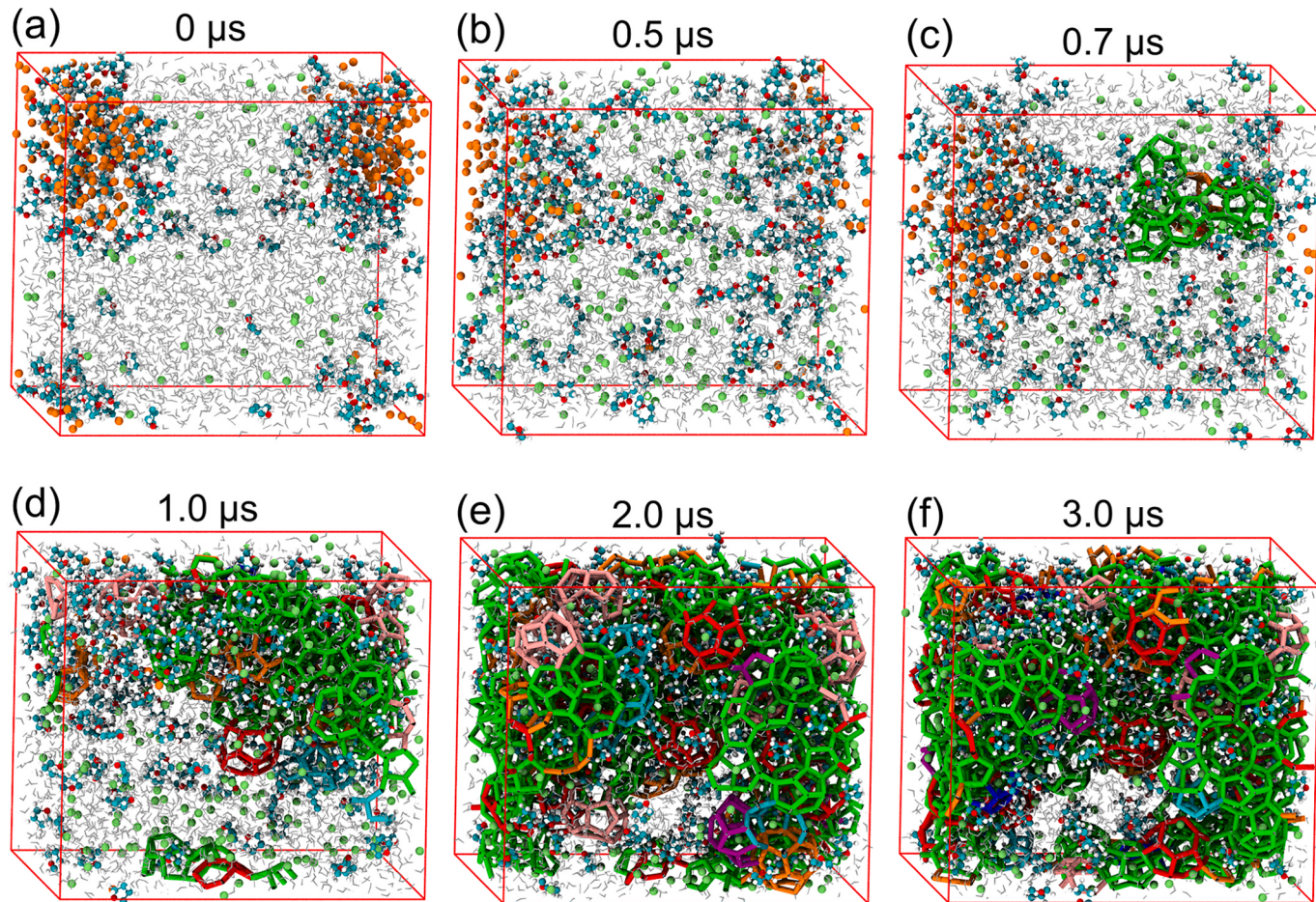


Fig. 4. Simulation snapshots showing the spontaneous nucleation process of binary $\text{H}_2\text{-THF}$ hydrates from two-phase solutions for the H_{THF} system at (a-f) different simulation times. THF is displayed as cyan (C atom), red (O atom), and white (H atom). Orange balls, green balls, and silver lines represent H_2 in nanobubble, H_2 in solution, and H_2O , respectively. Bonds of different colours represent seven types of hydrate cages, i.e., green for 5^{12} , blue for $5^{12}6^2$, red for $5^{12}6^3$, orange for $5^{12}6^4$, cyan for $4^{15}106^2$, purple for $4^{15}106^3$, and pink for $4^{15}106^4$. (For interpretation of the references to colour in this figure legend, the reader is referred to the web version of this article.)

beneficial for hydrate nucleation. The cage-faces in the cage-like hydrogen bond network absorb surrounding H_2 and THF molecules to stabilize their structures (Fig. 3(a-f)), which promotes the gradual transformation of the cage-like hydrogen bond network into a standard H_2 hydrate cage. At $0.615\ \mu\text{s}$ in the MD simulation, the hydrogen bond network begins to form around the guest molecules (THF and H_2) as shown in Fig. 3(a). The water molecules are arranged in a manner that starts to resemble the structure of a hydrate cage. In the time-window $0.618 - 0.625\ \mu\text{s}$, the hydrogen bond network becomes more defined as shown in Fig. 3(b-e). Water molecules continue to form hydrogen bonds, creating a more cage-like structure. After $0.631\ \mu\text{s}$ of simulation time, the hydrate cage structure appears to be well-formed, with H_2 molecules effectively being encapsulated in the cages as can be seen in Fig. 3(f). A large number of guest molecules (THF and H_2) are absorbed on the surface of the hydrate cage. This shows that the absorption of guest molecules on the cage-face is essential for hydrate nucleation. Our results support the cage adsorption hypothesis, in which hydrate cage-faces form first and then stabilize through guest molecule adsorption, rather than the mutually coordinated guest (MCG) mechanism, which suggests guest-driven cage formation. These insights contribute to a deeper understanding of hydrate nucleation pathways and may help in the development of strategies to enhance hydrate-based H_2 storage.

To quantitatively reveal the adsorption of guest molecules on the cage surface during the nucleation of binary H_2 hydrate, the time evolution of the number of guest molecules absorbed on cage-faces are

calculated. As shown in Fig. 5(a), each H_2 -occupied hydrate cage absorbs ca. 13 gas molecules (i.e., 8 H_2 and 5 THF molecules). More gas molecules are absorbed on the cage-faces of C_2H_6 -occupied and THF-occupied cages compared to CH_4 -occupied and CO_2 -occupied cages (see Fig. S9(a-h), S10(a-h), S11(a-h), and S12(a-h) in the Supplementary material). This difference can be attributed to the varying size and type of hydrate cages. As can be seen in Fig. 5(b), Fig. 5(c), Fig. S13(a-d) and Fig. S14(a-b) in the Supplementary material, during the first μs of the MD simulation ($0-1.0\ \mu\text{s}$), gas molecules gradually dissolve from the nanobubbles into the water, greatly increasing the concentration of guest molecules in water (Fig. 5(c)), and facilitating hydrate nucleation (see also Fig. S14(a-b) in the Supplementary material). Most of the promoter molecules in the $\text{H}_{\text{CH}4}$, $\text{H}_{\text{CO}2}$, $\text{H}_{\text{C}2\text{H}6}$, and $\text{H}_{\text{C}5\text{H}10}$ systems are in the solution or part of hydrates rather than in nanobubbles (see Fig. S14 (b) in the Supplementary material). During the second μs of the simulation ($1.0-2.0\ \mu\text{s}$), a large number of dissolved guest molecules in water are absorbed on the cage-faces, stabilizing the hydrate clusters, and thus, promoting hydrate nucleation (Fig. 5(b) and Fig. S13(a-d) in the Supplementary material). In the last μs of the simulation ($2.0-3.0\ \mu\text{s}$), most guest molecules dissolved in water are getting absorbed on the cage-faces, and only a few guest molecules remain in water (Fig. 5(b) and Fig. S13(a-d) in the Supplementary material). These findings indicate that the nucleation and growth of binary H_2 hydrates proceed in three stages: (1) guest molecules initially dissolve into water from the gas phase; (2) guest molecules dissolved in water are gradually absorbed on

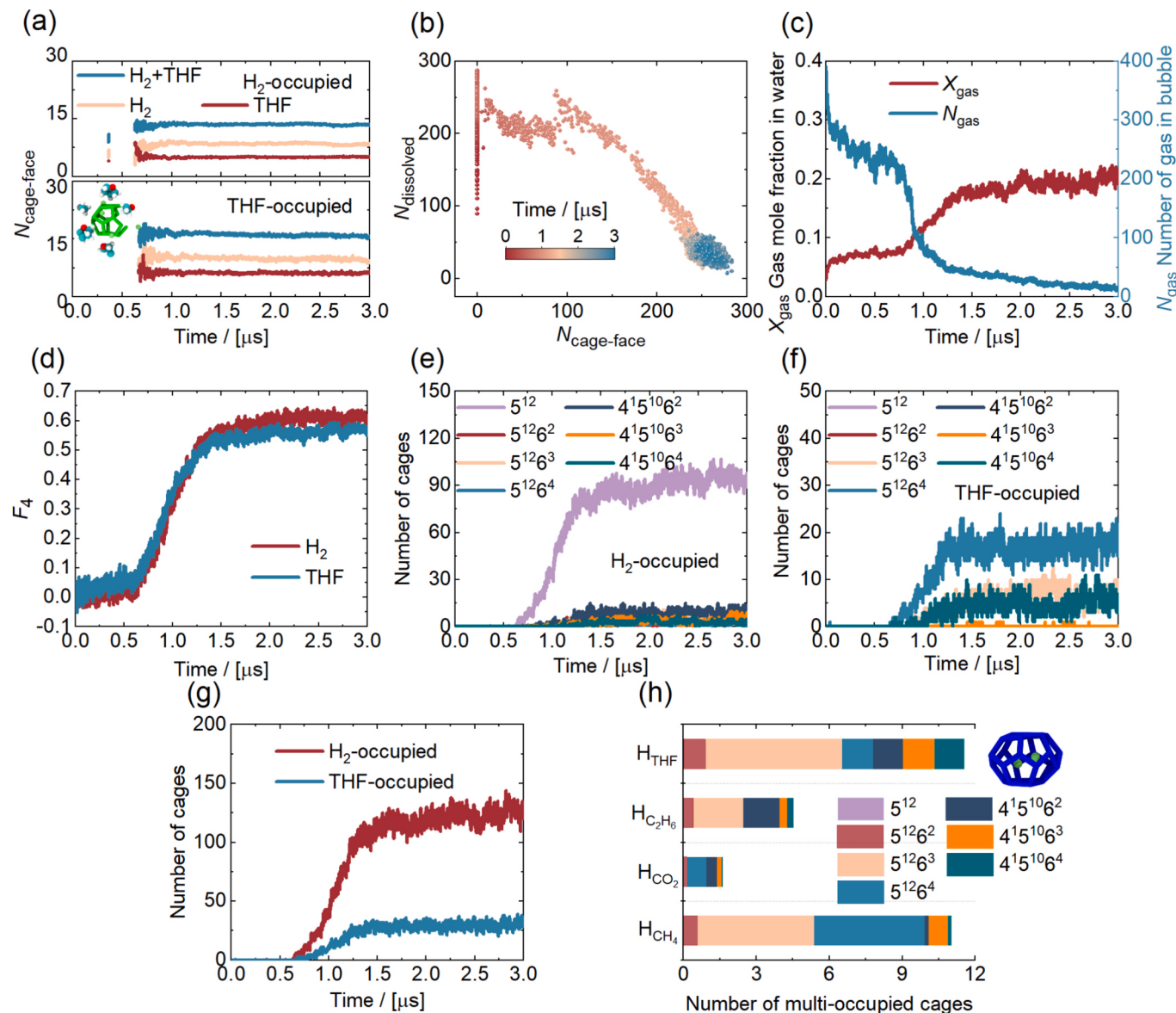


Fig. 5. (a) Time evolution of the number of gas H_2 and THF molecules ($N_{\text{cage-face}}$) absorbed to each face of the hydrate cage (i.e., cage-face) occupied by H_2 (H_2 -occupied) and THF (THF -occupied). (b) The number of gas molecules dissolved in water ($N_{\text{dissolved}}$) as a function of the number of gas molecules absorbed on cage-faces ($N_{\text{cage-face}}$). (c) Time evolution of the gas mole fraction x_{gas} in water and number of gas molecules in nanobubble N_{gas} . (d) Time evolution of the F_4 order parameters within 0.35 nm of H_2 and THF in water. Time evolution of the number of (e) H_2 -occupied cages, (f) THF -occupied cages, and (g) total hydrate cages. (h) The number of multi-occupied cages averaged over the last 0.1 μs of the simulation.

the cage-faces, promoting hydrate nucleation; and (3) most guest molecules in water are absorbed on the cage-faces, enhancing the stability and growth of binary H_2 hydrates. The spontaneous nucleation process of binary H_2 hydrates in the seven different systems studied here is shown in Videos S1-S7 provided as [Supplementary material](#).

The nucleation mechanism of binary H_2 hydrates is affected by the molecular size and diffusivity of the promoters. By the end of the simulations (after 3 μs), the formation of hydrate cages is not observed in the H_{Pure} , $H_{\text{C}_3\text{H}_8}$, and $H_{\text{C}_5\text{H}_{10}}$ systems. This can also be observed in the simulation snapshots shown in Fig. S15 in the [Supplementary material](#), where S15(a), (e), and (f) clearly contain only gas/liquid systems. This can be attributed to the gas–water two-phase setup used in this study, where the initial concentration of guest molecules in the water phase is much lower compared to the homogeneous solution systems commonly used in prior MD studies [50,52]. In homogeneous systems, most guest molecules are distributed in the water phase, significantly enhancing hydrate nucleation. Our previous study revealed that the higher the

concentration of guest molecules in the water phase, the more favorable it is for hydrate formation [68–70]. However, gas–water two-phase systems better mimic real hydrate nucleation conditions, making the results more relevant to practical applications. A maximum number of 25 C_3H_8 and C_5H_{10} molecules in the $H_{\text{C}_3\text{H}_8}$ and $H_{\text{C}_5\text{H}_{10}}$ systems are dissolved in water as shown in Fig. S14(b) in the [Supplementary material](#), where the gas mole fractions are illustrated as a function of simulation time. Most C_3H_8 and C_5H_{10} promoter molecules (>150) remain in the nanobubbles, and thus, are not available in the aqueous phase to form hydrates (Fig. S14(b) and S15(a, f) in the [Supplementary material](#)). The number of water molecules in the solution and in the hydrates as a function of time for the H_{CH_4} , H_{CO_2} , $H_{\text{C}_2\text{H}_6}$, and H_{THF} systems is shown in Fig. S16–S19 in the [Supplementary material](#). A large number of water molecules transition from liquid to hydrate with time in the H_{CH_4} , H_{CO_2} , $H_{\text{C}_2\text{H}_6}$, and H_{THF} systems as shown in Fig. S16(a-d), S17(a-d), S18(a-d), and S19(a-d) in the [Supplementary material](#).

The F_4 order parameter can accurately identify the state of water,

taking average values of -0.04 , -0.4 , and 0.7 for liquid water, ice, and hydrate, respectively [71]. The F_4 value computed in the vicinity of promoter molecules is higher than the respective quantity near H_2 molecules as shown in Fig. 5(d), S20(a-p), and S21(a-h) in the [Supplementary material](#). Due to their lower diffusivity compared to H_2 molecules [72], promoter molecules facilitate the formation of cage structures around them. As discussed earlier, both H_2 and promoter molecules can occupy hydrate cages as guest molecules. H_2 mainly occupies small cages (5^{12}) and a few large cages as shown in Fig. 5(e) and S22(a-p) in the [Supplementary material](#). Since CH_4 and CO_2 molecules (SI-type hydrate) are smaller than C_2H_6 and THF (SII-type hydrate), they mainly occupy small cages of 5^{12} and $4^{15}10^{6^2}$. C_2H_6 and THF molecules occupy large cages such as $5^{12}6^4$ (see Fig. 5(f) and S23(a-p)). However, during the last stages of nucleation in the H_{CH_4} system, we observed occasional instances where CH_4 molecules occupied large cages such as $5^{12}6^4$. This transient behavior is consistent with previous reports [73], where binary $\text{H}_2 + \text{CH}_4$ hydrates kinetically form SI structure hydrates first, with CH_4 molecules occupying small and large cages, before transitioning to the thermodynamically stable SII structure hydrate. This dynamic behavior reflects the interplay between kinetic and thermodynamic factors during hydrate nucleation. The number of H_2 -occupied hydrate cages exceeds that of promoter-occupied hydrate cages in the $\text{H}_{\text{C}_2\text{H}_6}$ and H_{THF} systems (see Fig. 5(g), S24(a-d), and S25(a-d) in the [Supplementary material](#)), which enhances the storage capacity of H_2 in clathrate hydrates.

H_2 hydrate cages that are occupied by multiple guest molecules (*i.e.*, multi-occupied H_2 hydrate cages) are frequently observed during the nucleation processes of binary H_2 hydrates, which have also been observed in previous MD studies [44]. The number of multi-occupied cages is the highest in the H_{THF} system, followed by the H_{CH_4} , $\text{H}_{\text{C}_2\text{H}_6}$,

and H_{CO_2} systems as shown in Fig. 5(h). As can be seen in Fig. 5(h) and S26(a-d) in the [Supplementary material](#), these multi-occupied hydrate cages are mainly large $5^{12}6^3$ and $5^{12}6^4$ cages, with a small number of $4^{15}10^{6^3}$ and $4^{15}10^{6^4}$ cages. More large hydrate cages are formed in the presence of large-sized promoter molecules (Fig. S23(a-p) and S24(a-p)), which enhances the formation of multi-occupied hydrate cages. Multi-occupied H_2 hydrate cages can theoretically store more H_2 molecules than H_2 hydrate cages that are occupied by single H_2 molecules. Therefore, the formation of more multi-occupied H_2 hydrate cages is beneficial for the H_2 storage in clathrate hydrates.

3.3. The effect of promoter species on H_2 storage in clathrate hydrates

Different promoter species affect H_2 storage in clathrate hydrate in a unique manner. This is also manifested in the so-called hydrate induction time which is the time it takes for H_2 and promoter species to transform from the gas phase to hydrates. Short induction times indicate fast H_2 hydrate nucleation, which is beneficial for H_2 storage. Although the induction time in the $\text{H}_{\text{C}_2\text{H}_6}$ and H_{THF} systems is slightly longer compared to H_{CH_4} and H_{CO_2} , it is much shorter than that in the H_{Pure} , $\text{H}_{\text{C}_3\text{H}_8}$, and $\text{H}_{\text{C}_5\text{H}_{10}}$ systems as shown in Fig. 6(a) and Fig. S27(a-g) in the [supplementary material](#). From the last 100 ns of the simulations, when the final stages of binary H_2 hydrate nucleation and growth are taking place, it is shown that ca. 47 % of H_2 is converted from the gas phase to hydrates in the H_{THF} system. This practically means that 47 % of the total H_2 molecules in the system are stored in the clathrate hydrate (see Fig. 6(b)). In contrast, 29.63 %, 25.99 %, and 8 % of the total H_2 are stored in hydrates for the H_{CH_4} , $\text{H}_{\text{C}_2\text{H}_6}$, and H_{CO_2} systems, respectively, while no H_2 is stored in hydrates in the H_{Pure} , $\text{H}_{\text{C}_3\text{H}_8}$, and $\text{H}_{\text{C}_5\text{H}_{10}}$ systems (see Fig. 6(b)). This shows that the H_2 storage capacity in the H_{THF}

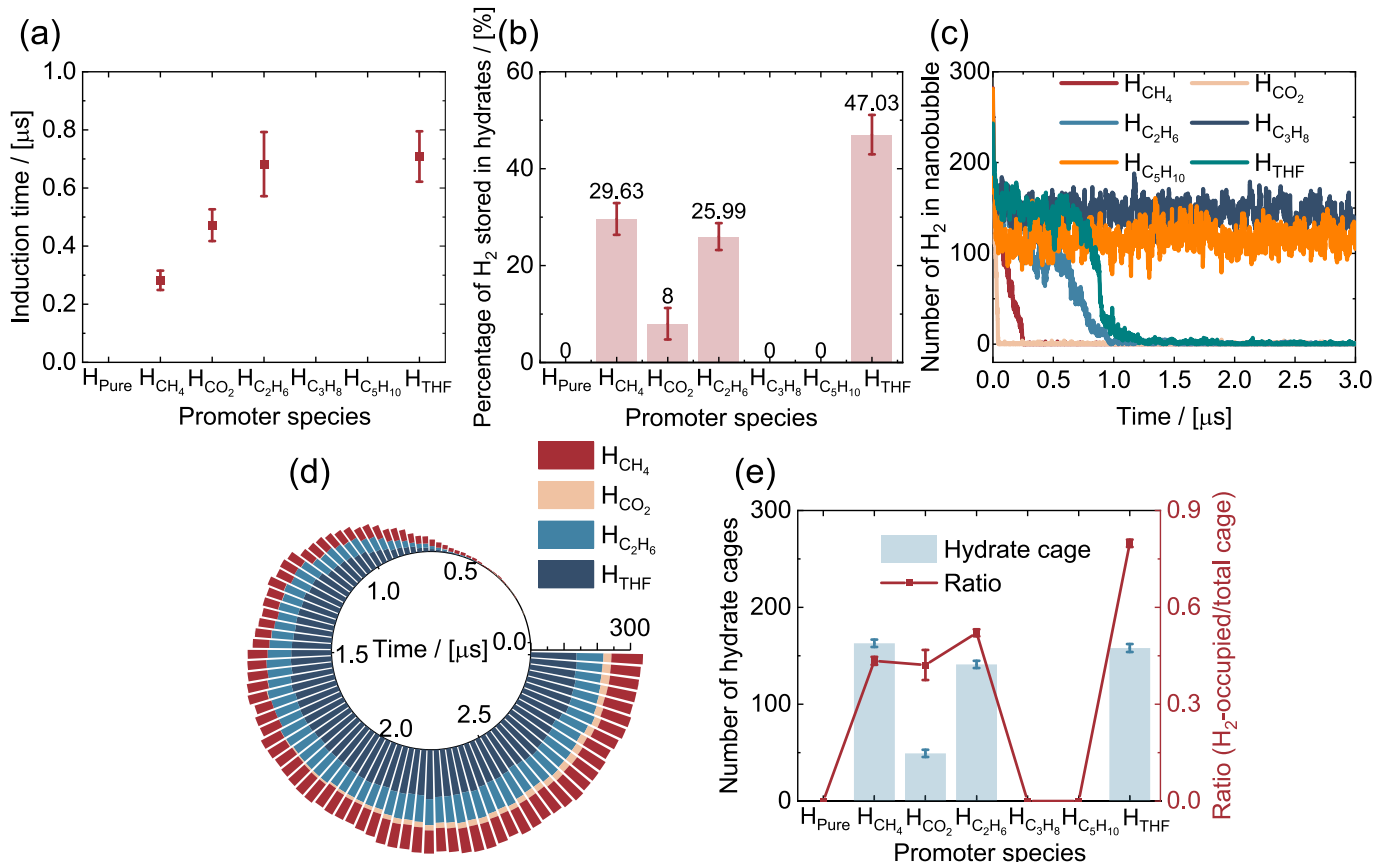


Fig. 6. (a) Induction time of hydrate nucleation with various promoters. (b) The percentage of H_2 storage (number of H_2 in hydrate/total) with various promoters averages the last 0.1 μs . Time evolution of the number of (c) H_2 in nanobubbles and (d) H_2 in hydrates. (e) The number of total hydrate cages and the number ratio (H_2 -occupied/total cages) average the last 0.1 μs for the seven systems, *i.e.*, H_{Pure} , H_{CH_4} , H_{CO_2} , $\text{H}_{\text{C}_2\text{H}_6}$, $\text{H}_{\text{C}_3\text{H}_8}$, $\text{H}_{\text{C}_5\text{H}_{10}}$, and H_{THF} .

system is the highest among the systems studied (also see Fig. S28 in the [supplementary material](#)), indicating that THF is the most beneficial promoter for the storage capacity of H₂ in clathrate hydrate. In contrast, a large number of H₂ molecules remain in nanobubbles, and thus, cannot be stored in clathrate hydrates for the H_{C3H8} and H_{C5H10} systems as shown in Fig. 6(c) and S29(a-g) in the [supplementary material](#). Therefore, C₃H₈ and C₅H₁₀ molecules are less effective promoters for converting H₂ from the gas phase to hydrate.

To further reveal the effect of different promoters on the H₂ storage capacity, the time evolution of the number of H₂ in clathrate hydrates in different systems is calculated and shown in Fig. 6(d). During the simulation period of 3 μs, the H₂ storage capacity in the H_{CH4}, H_{CO2}, H_{C2H6}, and H_{THF} systems gradually increases. As shown in Fig. 6(d) and S28 in the [supplementary material](#), the H₂ storage capacity in the H_{CO2} system is low, while it is high in the H_{THF} system. The H₂ storage capacities of the H_{CH4} and H_{C2H6} systems fall in between H_{CO2} and H_{THF}. From the last 100 ns of the simulations, it is shown that the total number of hydrate cages in the H_{CH4}, H_{C2H6}, and H_{THF} systems does not significantly differ from each other (Fig. 6(e) and S30 in the [supplementary material](#)). The proportion of H₂-occupied hydrate cages in the H_{THF} system reaches 0.8, which is much higher compared to the rest of the systems (Fig. 6(e)). The total number of hydrate cages in the H_{CO2} system is small (see Fig. 6(e)), and the proportion of H₂-occupied hydrate cages in the H_{CO2} system is lower compared to the rest of the systems (Fig. 6(e) and S30 in the [supplementary material](#)). Our findings clearly show that, among the species studied, THF is the most effective promoter for H₂ storage in clathrate hydrates, exhibiting high performance in converting H₂ from the gas phase to hydrate.

A systematic experimental investigation to reveal the effect of promoter species on H₂ hydrate formation is largely lacking. By comparing the available experimental data, we observe that the highest density of hydrogen can be obtained when THF is used as a promoter [19,74,75]. As a future outlook, novel efficient promoters for H₂ storage in hydrates could possibly be discovered based guided by the beneficial characteristics of THF molecules (which exhibit high Gibbs free energy and slow diffusivity in water). By monitoring these properties via MD simulations, one can efficiently screen and design superior H₂ hydrate promoters. This approach will not only expedite the identification of potential promoters but also provide theoretical references for subsequent experimental validation. In a follow up study, we focus on systematic screening of new promoter classes to optimize H₂ storage efficiency and environmental compatibility.

3.4. Integrated mechanistic framework for hydrate nucleation

While previous sections have analyzed individual properties influencing hydrate nucleation, it is essential to consider how these factors collectively control the nucleation mechanism. The Gibbs free energy of solvation influences guest molecule availability, which, together with molecular mobility (diffusivity), dictates transport to pre-nucleation sites. A longer residence time of guest molecules near water clusters stabilizes incipient hydrate structures, facilitating nucleation. A shorter residence time suggests rapid molecular exchange, preventing stable cage formation. A sufficiently long residence time allows for stronger molecular interactions between guest molecules and the hydrogen bond network, facilitating cage stabilization and hydrate nucleation. However, an excessively long residence time may indicate low diffusivity, limiting mass transfer to pre-nucleation sites. Hydrogen bond formation between water molecules dictates the stability of pre-nucleation clusters. Stronger hydrogen bonding networks lead to more rigid water structures, facilitating cage formation and reducing the likelihood of premature cluster dissociation. Our findings highlight that successful hydrate nucleation requires a balance between solubility (free energy), molecular mobility (diffusivity), and local structuring effects (residence time and hydrogen bonding). For instance, while CH₄ exhibits a less negative solvation free energy than THF due to its smaller molecule size

and hydrophobic interactions, THF simultaneously promotes longer residence times and more stable hydrogen bonding networks. This multi-faceted stabilization explains its superior performance in binary H₂ hydrate nucleation. This physics-informed analysis serves as a framework for assessing promoter efficiency, based on which novel promoters can be evaluated.

3.5. Implications for hydrogen storage and the search for novel promoters

Hydrate-based H₂ storage is a promising alternative to traditional gas and liquid-phase storage methods, offering advantages in safety and energy efficiency. However, several challenges remain, including low formation rates, limited storage capacities, and the need for stable and environmentally friendly promoters. While THF is an effective promoter, but its volatility and potential toxicity limit its practical applications. CO₂, another widely studied promoter, raises concerns due to its environmental effect. Hydrocarbon-based promoters such as CH₄, C₂H₆, and C₃H₈ exhibit moderate promoting effects but contribute to greenhouse gas emissions and present safety concerns. The ideal hydrate promoter should possess: (1) High solubility in water to maximize guest molecule availability; (2) Optimized residence time to enhance nucleation without excessive mobility; (3) Strong hydrogen bonding interactions to facilitate stable cage formation; (4) Environmental sustainability to minimize ecological impact. Functionalized organic molecules, ionic liquids (ILs), and nanoparticle-assisted nucleation have been expected to influence hydrate nucleation and could serve as novel, tunable promoters. In the future, we focus on systematic screening of these new promoter classes to optimize H₂ storage efficiency and environmental compatibility. Our study clearly shows that THF is the most effective promoter under the simulated conditions, a finding that is in line with prior studies. To advance the field, future research should focus on identifying novel promoters with enhanced performance, improved environmental profiles, and/or unique molecular functionalities. Potential candidates include functionalized organic molecules, ionic liquids, and nanoparticle-assisted systems. In this context, the quantitative framework presented here (linking solvation free energy, diffusivity, hydrogen bonding, and residence time) provides clear criteria for evaluating and designing new promoters. Such an approach could lead to the discovery of additives that not only match but potentially surpass THF in promoting hydrate-based hydrogen storage.

4. Conclusions

An extensive series of μs-scale molecular dynamics simulations are performed to investigate the nucleation of binary H₂ hydrates from the gas-liquid two-phase solution in the presence of various promoter molecules, i.e., CH₄, CO₂, C₂H₆, C₃H₈, C₅H₁₀, and THF. The simulation results show that the H₂ and promoter molecules first dissolve in water from the gas phase and then are absorbed on the cage-faces, promoting the nucleation and growth of binary H₂ hydrates. Promoter molecules, due to their lower diffusivity compared to H₂ molecules, facilitate the formation of cage structures near the promoter molecules. The nucleation of binary H₂ hydrates is affected by the molecular size and diffusivity of the promoters. THF has low diffusivity in water and can occupy many of the large hydrate cages, characteristics that are beneficial for H₂ storage in clathrate hydrates. Therefore, THF (followed by CH₄, C₂H₆, and CO₂) is the most effective promoter for H₂ storage in clathrate hydrate, exhibiting high performance in converting H₂ from the gas phase to hydrates. C₃H₈ and C₅H₁₀ molecules are less efficient H₂ hydrate promoters. H₂ molecules mainly occupy small hydrate cages, while promoter molecules occupy various cages depending on their molecular size. The multi-occupied hydrate cages are mainly large cages of 5¹²6³ and 5¹²6⁴. The presence of large-sized promoters enhances the formation of the multi-occupied hydrate cage. The molecular insight provided here into the nucleation of binary H₂ hydrates with various promoters contributes to a broader understanding of hydrate-based H₂ storage. We

are confident that this investigation is poised to catalyse further experimental and computational research efforts, particularly in developing new promoters for H₂ hydrate formation, and providing theoretical guidelines for experiments.

CRediT authorship contribution statement

Fengyi Mi: Writing – review & editing, Writing – original draft, Visualization, Validation, Software, Methodology, Investigation, Formal analysis, Data curation, Conceptualization. **Fulong Ning:** Writing – review & editing, Writing – original draft, Supervision, Resources, Methodology, Funding acquisition, Conceptualization. **Thijs J.H. Vlugt:** Data curation. **Othonas A. Moultsos:** Data curation.

Declaration of competing interest

The authors declare that they have no known competing financial interests or personal relationships that could have appeared to influence the work reported in this paper.

Acknowledgements

This work was supported by the National Science Foundation for Distinguished Young Scholars (42225207), Natural Science Foundation of Hubei Province (2021CFA024), and China Scholarship Council (CSC202306410133). The authors acknowledge the use of computational resources of DelftBlue supercomputer, provided by Delft High Performance Computing Centre (<https://www.tudelft.nl/dhpc>).

Appendix A. Supplementary material

Supplementary data to this article can be found online at <https://doi.org/10.1016/j.cej.2025.162253>.

Data availability

Data will be made available on request.

References

- [1] M. Momirlan, T. Veziroglu, Current status of hydrogen energy, *Renew. Sustain. Energy Rev.* 6 (1–2) (2002) 141–179.
- [2] T. Zhang, J. Uratani, Y. Huang, L. Xu, S. Griffiths, Y. Ding, Hydrogen liquefaction and storage: recent progress and perspectives, *Renew. Sustain. Energy Rev.* 176 (2023) 113204.
- [3] M.I. Khan, T. Yasmin, A. Shakoor, Technical overview of compressed natural gas (CNG) as a transportation fuel, *Renew. Sustain. Energy Rev.* 51 (2015) 785–797.
- [4] P. Habibi, T.H. Saji, T.J.H. Vlugt, O.A. Moultsos, P. Dey, Hydrogen dissociation in Li-decorated borophene and borophene hydride: an ab-initio study, *Appl. Surf. Sci.* 603 (2022) 154323.
- [5] P. Habibi, T.J.H. Vlugt, P. Dey, O.A. Moultsos, Reversible hydrogen storage in metal-decorated honeycomb borophene oxide, *ACS Appl. Mater. Interfaces* 13 (36) (2021) 43233–43240.
- [6] L.S. Blankenship, N. Balahmar, R. Mokaya, Oxygen-rich microporous carbons with exceptional hydrogen storage capacity, *Nat. Commun.* 8 (1) (2017) 1545.
- [7] E.S. Cho, A.M. Ruminski, S. Aloni, Y.-S. Liu, J. Guo, J.J. Urban, Graphene oxide/metal nanocrystal multilaminates as the atomic limit for safe and selective hydrogen storage, *Nat. Commun.* 7 (1) (2016) 10804.
- [8] P. Jena, Materials for hydrogen storage: past, present, and future, *J. Phys. Chem. Lett.* 2 (3) (2011) 206–211.
- [9] S. Niaz, T. Manzoor, A.H. Pandith, Hydrogen storage: materials, methods and perspectives, *Renew. Sustain. Energy Rev.* 50 (2015) 457–469.
- [10] H. Lee, J.W. Lee, D.Y. Kim, J. Park, Y.T. Seo, H. Zeng, I.L. Moudrakovski, C. I. Ratcliffe, J.A. Ripmeester, Tuning clathrate hydrates for hydrogen storage, *Nature* 434 (7034) (2005) 743–746.
- [11] W.L. Mao, H.K. Mao, Hydrogen storage in molecular compounds, *Proc. Nat. Acad. Sci. USA* 101 (3) (2004) 708–710.
- [12] W.L. Mao, H.K. Mao, A.F. Goncharov, V.V. Struzhkin, Q. Guo, J. Hu, J. Shu, R. J. Hemley, M. Somayazulu, Y. Zhao, Hydrogen clusters in clathrate hydrate, *Science* 297 (5590) (2002) 2247–2249.
- [13] E.D. Sloan Jr., Fundamental principles and applications of natural gas hydrates, *Nature* 426 (6964) (2003) 353–359.
- [14] V.V. Struzhkin, B. Militzer, W.L. Mao, H.K. Mao, R.J. Hemley, Hydrogen storage in molecular clathrates, *Chem. Rev.* 107 (10) (2007) 4133–4151.
- [15] J. Wu, F. Ning, T.T. Trinh, S. Kjelstrup, T.J.H. Vlugt, J. He, B.H. Skallerud, Z. Zhang, Mechanical instability of monocrystalline and polycrystalline methane hydrates, *Nat. Commun.* 6 (1) (2015) 8743.
- [16] X. Kou, X.S. Li, Y. Wang, R. Xu, Z.Y. Chen, Macroscale insights into heterogeneous hydrate formation and decomposition behaviors in porous media, *Chem. Eng. J.* 475 (2023) 146215.
- [17] B.J. Cao, Y.F. Sun, H.N. Chen, J.R. Zhong, M.L. Wang, M.Y. Niu, J.Y. Kan, C.Y. Sun, D.Y. Chen, G.J. Chen, An approach to the high efficient exploitation of nature gas hydrate and carbon sequestration via injecting CO₂/H₂ gas mixture with varying composition, *Chem. Eng. J.* 455 (2023) 140634.
- [18] N. Papadimitriou, I. Tsipanogiannis, A.T. Papaioannou, A. Stubos, Evaluation of the hydrogen-storage capacity of pure H₂ and binary H₂-THF hydrates with Monte Carlo simulations, *J. Phys. Chem. C* 112 (27) (2008) 10294–10302.
- [19] A. Davoodabadi, A. Mahmoudi, H. Ghasemi, The potential of hydrogen hydrate as a future hydrogen storage medium, *Iscience* 24 (1) (2021).
- [20] Y. Zhang, G. Bhattacharjee, R. Kumar, P. Linga, Solidified hydrogen storage (Solid-HyStore) via clathrate hydrates, *Chem. Eng. J.* 431 (2022) 133702.
- [21] N.N. Nguyen, Prospect and challenges of hydrate-based hydrogen storage in the low-carbon future, *Energ. Fuels* 37 (14) (2023) 9771–9789.
- [22] A. Gupta, G.V. Baron, P. Perreault, S. Lenaerts, R.-G. Ciocarlan, P. Cool, P.G. Mileo, S. Rogge, V. Van Speybroeck, G. Watson, Hydrogen clathrates: Next generation hydrogen storage materials, *Energy Storage Mater.* 41 (2021) 69–107.
- [23] T. Sugahara, J.C. Haag, P.S. Prasad, A.A. Warntjes, E.D. Sloan, A.K. Sum, C.A. Koh, Increasing hydrogen storage capacity using tetrahydrofuran, *J. Am. Chem. Soc.* 131 (41) (2009) 14616–14617.
- [24] H.P. Veluswamy, R. Kumar, P. Linga, Hydrogen storage in clathrate hydrates: current state of the art and future directions, *Appl. Energy* 122 (2014) 112–132.
- [25] R. Firuznia, A. Abutalib, A. Hakimian, S. Nazifi, Z. Huang, T.R. Lee, J.D. Rimer, H. Ghasemi, High-capacity hydrogen storage through molecularly restructured and confined hydrogen hydrates, *Mater. Today Phys.* 38 (2023) 101248.
- [26] Y. Zhang, G. Bhattacharjee, J. Zheng, P. Linga, Hydrogen storage as clathrate hydrates in the presence of 1, 3-dioxolane as a dual-function promoter, *Chem. Eng. J.* 427 (2022) 131771.
- [27] P. Wang, Y. Chen, Y. Teng, S. An, Y. Li, M. Han, B. Yuan, S. Shen, B. Chen, S. Han, A comprehensive review of hydrogen purification using a hydrate-based method, *Renew. Sustain. Energy Rev.* 194 (2024) 114303.
- [28] N.I. Papadimitriou, I.N. Tsipanogiannis, I.G. Economou, A.K. Stubos, Storage of H₂ in clathrate hydrates: evaluation of different force-fields used in Monte Carlo simulations, *Mol. Phys.* 115 (9–12) (2017) 1274–1285.
- [29] N.I. Papadimitriou, I.N. Tsipanogiannis, I.G. Economou, A.K. Stubos, The effect of lattice constant on the storage capacity of hydrogen hydrates: a Monte Carlo study, *Mol. Phys.* 114 (18) (2016) 2664–2671.
- [30] I.N. Tsipanogiannis, I.G. Economou, Monte Carlo simulation studies of clathrate hydrates: A review, *J. Supercrit. Fluids* 134 (2018) 51–60.
- [31] A. Chapoy, R. Anderson, B. Tohid, Low-pressure molecular hydrogen storage in semi-clathrate hydrates of quaternary ammonium compounds, *J. Am. Chem. Soc.* 129 (4) (2007) 746–747.
- [32] Y. Guo, W. Wu, B. Hao, Q. Zheng, Formation of hydrogen hydrate in the presence of thermodynamic promoters: a review and prospects, *Int. J. Hydrogen Energy* 60 (2024) 1462–1480.
- [33] W. Lee, D.W. Kang, Y.-H. Ahn, J.W. Lee, Blended hydrate seed and liquid promoter for the acceleration of hydrogen hydrate formation, *Renew. Sustain. Energy Rev.* 177 (2023) 113217.
- [34] S. Chen, Y. Wang, X. Lang, S. Fan, G. Li, Rapid and high hydrogen storage in epoxycyclopentane hydrate at moderate pressure, *Energy* 268 (2023) 126638.
- [35] Y.N. Kong, F. Wang, G.D. Zhang, X.L. Wang, Enhanced formation kinetics of mixed H₂/THF hydrate in the presence of nano promoters, *Chem. Eng. J.* 474 (2023) 145901.
- [36] L.J. Florusse, C.J. Peters, J. Schoonman, K.C. Hester, C.A. Koh, S.F. Dec, K. N. Marsh, E.D. Sloan, Stable low-pressure hydrogen clusters stored in a binary clathrate hydrate, *Science* 306 (5695) (2004) 469–471.
- [37] T.A. Strobel, C.J. Taylor, K.C. Hester, S.F. Dec, C.A. Koh, K.T. Miller, E.D. Sloan Jr., Molecular hydrogen storage in binary THF-H₂ clathrate hydrates, *J. Phys. Chem. B* 110 (34) (2006) 17121–17125.
- [38] Y.-H. Ahn, S. Moon, D.-Y. Koh, S. Hong, H. Lee, J.W. Lee, Y. Park, One-step formation of hydrogen clusters in clathrate hydrates stabilized via natural gas blending, *Energy Storage Mater.* 24 (2020) 655–661.
- [39] Y. Kong, H. Yu, M. Liu, G. Zhang, F. Wang, Ultra-rapid formation of mixed H₂/DIOX/THF hydrate under low driving force: Important insight for hydrate-based hydrogen storage, *Appl. Energy* 362 (2024) 123029.
- [40] J. Zhang, Y. Li, Z. Yin, X.Y. Zheng, P. Linga, How THF tunes the kinetics of H₂-THF hydrates? a kinetic study with morphology and calorimetric analysis, *Ind. Eng. Chem. Res.* 62 (51) (2023) 21918–21932.
- [41] J. Farrando-Perez, R. Balderas-Xicotencatl, Y. Cheng, L. Daemen, C. Cuadrado-Collados, M. Martinez-Escandell, A.J. Ramirez-Cuesta, J. Silvestre-Albero, Rapid and efficient hydrogen clathrate hydrate formation in confined nanospace, *Nat. Commun.* 13 (1) (2022) 5953.
- [42] W. Lee, D.W. Kang, Y.-H. Ahn, J.W. Lee, Rapid formation of hydrogen-enriched hydrocarbon gas hydrates under static conditions, *ACS Sustain. Chem. Eng.* 9 (25) (2021) 8414–8424.
- [43] J. Zhang, Y. Li, Z. Yin, P. Linga, T. He, X.Y. Zheng, Coupling amino acid L-Val with THF for superior hydrogen hydrate kinetics: implication for hydrate-based hydrogen storage, *Chem. Eng. J.* 467 (2023) 143459.
- [44] S. Alavi, J.A. Ripmeester, D.D. Klug, Molecular-dynamics study of structure II hydrogen clathrates, *J. Chem. Phys.* 123 (2) (2005) 24507.

- [45] B. Fang, O.A. Moults, T. Lü, J. Sun, Z. Liu, F. Ning, T.J.H. Vlugt, Effects of nanobubbles on methane hydrate dissociation: a molecular simulation study, *Fuel* 345 (2023) 128230.
- [46] F. Mi, Z. He, F. Ning, Molecular insight on CO₂/C₃H₈ mixed hydrate formation from the brine for sustainable hydrate-based desalination, *Sep. Purif. Technol.* 353 (2025) 128244.
- [47] Y. Chen, X. Zhou, C. Tang, X. Zang, J. Guan, J. Lu, D. Liang, Molecular insight into the dual effect of salts: Promoting or inhibiting the nucleation and growth of carbon dioxide clathrate hydrates, *Chem. Eng. J.* 155097 (2024).
- [48] Y. Lu, C.Y. Yuan, H. Wang, L. Yang, L.X. Zhang, J.F. Zhao, Y.C. Song, Atomistic insights into the performance of thermodynamic inhibitors in the nucleation of methane hydrate, *Chem. Eng. J.* 431 (2022) 133479.
- [49] P. Wang, H. Long, Y. Teng, Y. Li, Y. Li, J. Zhu, H. Xie, S. Han, Y. Zhao, J. Zhu, Investigation of hydrogen-propane hydrate formation mechanism and optimal pressure range via hydrate-based hydrogen storage, *Fuel* 361 (2024) 130791.
- [50] W. Bao, Y. Teng, P. Wang, Y. Li, J. Zhu, S. Han, J. Zhu, H. Xie, Y. Zhao, Molecular analysis of hydrogen-propane hydrate formation mechanism and its influencing factors for hydrogen storage, *Int. J. Hydrogen Energy* 50 (2024) 697–708.
- [51] P.F. Wang, K.H. Li, J.Y. Yang, J.L. Zhu, Y.S. Zhao, Y. Teng, Experimental and theoretical study on dissociation thermodynamics and kinetics of hydrogen-propane hydrate, *Chem. Eng. J.* 426 (2021) 131279.
- [52] Y. Wang, K. Yin, X. Lang, S. Fan, G. Li, C. Yu, S. Wang, Hydrogen storage in sH binary hydrate: insights from molecular dynamics simulation, *Int. J. Hydrogen Energy* 46 (29) (2021) 15748–15760.
- [53] W. Hu, X. Tian, C. Chen, C. Cheng, S. Zhu, J. Zhang, T. Qi, T. Jin, X. Wu, Molecular dynamic simulation of H₂-CH₄ binary hydrate growth induced by methane hydrate, *Fuel* 360 (2024) 130554.
- [54] D.W. Kang, W. Lee, Y.-H. Ahn, J.W. Lee, Exploring tuning phenomena of THF-H₂ hydrates via molecular dynamics simulations, *J. Mol. Liq.* 349 (2022) 118490.
- [55] Y. Wang, K. Yin, S. Fan, X. Lang, C. Yu, S. Wang, S. Li, The molecular insight into the “Zeolite-ice” as hydrogen storage material, *Energy* 217 (2021) 119406.
- [56] J. Xu, X. Yang, J. Chen, Z. Meng, X. Wang, B. Wang, J. Wang, Y. Wang, J. Qu, Y. Qi, Molecular study on the growth mechanism of CO₂-H₂ binary hydrate promoted by electric field, *Fuel* 363 (2024) 130924.
- [57] K.C. Sloan ED, *Clathrate Hydrates of Natural Gases*, CRC Press, Boca Raton, FL, 2008.
- [58] W.L. Jorgensen, D.S. Maxwell, J. TiradoRives, Development and testing of the OPLS all-atom force field on conformational energetics and properties of organic liquids, *J. Am. Chem. Soc.* 118 (45) (1996) 11225–11236.
- [59] J.J. Potoff, J.I. Siepmann, Vapor-liquid equilibria of mixtures containing alkanes, carbon dioxide, and nitrogen, *AIChE J.* 47 (7) (2001) 1676–1682.
- [60] J.L. Abascal, E. Sanz, R. García Fernandez, C. Vega, A potential model for the study of ices and amorphous water: TIP4P/Ice, *J. Chem. Phys.* 122 (23) (2005) 234511.
- [61] F. Mi, Z. He, G. Jiang, F. Ning, Effect of glucose on CH₄ hydrate formation in Clay nanopores and bulk solution: insights from microsecond molecular dynamics simulations, *ACS Sustain. Chem. Eng.* 12 (11) (2024) 4644–4654.
- [62] S. Nose, A molecular-dynamics method for simulations in the canonical ensemble, *Mol. Phys.* 52 (2) (1984) 255–268.
- [63] M. Parrinello, A. Rahman, Crystal structure and pair potentials: a molecular-dynamics study, *Phys. Rev. Lett.* 45 (14) (1980) 1196–1199.
- [64] M.J. Abraham, T. Murtola, R. Schulz, S. Päll, J.C. Smith, B. Hess, E. Lindahl, GROMACS: High performance molecular simulations through multi-level parallelism from laptops to supercomputers, *SoftwareX* 1 (2015) 19–25.
- [65] M.R. Shirts, J.W. Pitera, W.C. Swope, V.S. Pande, Extremely precise free energy calculations of amino acid side chain analogs: comparison of common molecular mechanics force fields for proteins, *J. Chem. Phys.* 119 (11) (2003) 5740–5761.
- [66] B. Fang, P. Habibi, O.A. Moults, T. Lü, F. Ning, T.J.H. Vlugt, Solubilities and self-diffusion coefficients of light n-alkanes in NaCl solutions at the temperature range (278.15–308.15) K and pressure range (1–300) bar and thermodynamics properties of their corresponding hydrates at (150–290) K and (1–7000) bar, *J. Chem. Eng. Data* (2023).
- [67] Z. Zhang, P.G. Kusalik, G.-J. Guo, Molecular insight into the growth of hydrogen and methane binary hydrates, *J. Phys. Chem. C* 122 (14) (2018) 7771–7778.
- [68] F. Mi, Z. He, Y. Zhao, G. Jiang, F. Ning, Effects of surface property of mixed clays on methane hydrate formation in nanopores: a molecular dynamics study, *J. Colloid Interface Sci.* 627 (2022) 681–691.
- [69] F.Y. Mi, W. Li, J.T. Pang, O.A. Moults, F.L. Ning, T.J.H. Vlugt, Molecular insights into the microscopic behavior of CO₂ hydrates in oceanic sediments: implications for carbon sequestration, *J. Phys. Chem. C* 128 (43) (2024) 18588–18597.
- [70] F. Mi, J. Pang, W. Li, O.A. Moults, F. Ning, T.J.H. Vlugt, Novel pseudo-hexagonal montmorillonite model and microsecond MD simulations of hydrate formation in mixed clay sediments with surface defects, *J. Chem. Phys.* 161 (21) (2024).
- [71] L.A. Báez, P. Clancy, Computer Simulation of the Crystal Growth and Dissolution of Natural Gas Hydrates, *Ann. N.Y. Acad. Sci.* 715(1 Natural Gas H) (1994) 177–186.
- [72] I.N. Tsipanogiannis, S. Maity, A.T. Celebi, O.A. Moults, Engineering model for predicting the intradiffusion coefficients of hydrogen and oxygen in vapor, liquid, and supercritical water based on molecular dynamics simulations, *J. Chem. Eng. Data* 66 (8) (2021) 3226–3244.
- [73] Y. Matsumoto, R.G. Grim, N.M. Khan, T. Sugahara, K. Ohgaki, E.D. Sloan, C.A. Koh, A.K. Sum, Investigating the thermodynamic stabilities of hydrogen and methane binary gas hydrates, *J. Phys. Chem. C* 118 (7) (2014) 3783–3788.
- [74] J. Cai, Y.Q. Tao, N. von Solms, C.G. Xu, Z.Y. Chen, X.S. Li, Experimental studies on hydrogen hydrate with tetrahydrofuran by differential scanning calorimeter and in-situ Raman, *Appl. Energy* 243 (2019) 1–9.
- [75] T. Sugahara, J.C. Haag, A.A. Warnajes, P.S.R. Prasad, E.D. Sloan, C.A. Koh, A. K. Sum, Large-cage occupancies of hydrogen in binary clathrate hydrates dependent on pressures and guest concentrations, *J. Phys. Chem. C* 114 (35) (2010) 15218–15222.